Published in final edited form as:
J Neurosci Methods. 2012 October 15; 211(1): 22–30. doi:10.1016/j.jneumeth.2012.08.005.

Variability of acute extracellular action potential measurements with multisite silicon probes

Kimberly M. Scott[1,2,3], **Jiangang Du**[1,2], **Henry A. Lester**[1], and **Sotiris C. Masmanidis**[1,2,4,*]
[1]Division of Biology, California Institute of Technology, Pasadena, USA
[2]Broad Fellows Program in Brain Circuitry, California Institute of Technology, Pasadena, USA

Abstract

Device miniaturization technologies have led to significant advances in sensors for extracellular measurements of electrical activity in the brain. Multisite, silicon-based probes containing implantable electrode arrays afford greater coverage of neuronal activity than single electrodes and therefore potentially offer a more complete view of how neuronal ensembles encode information. However, scaling up the number of sites is not sufficient to ensure capture of multiple neurons, as action potential signals from extracellular electrodes may vary due to numerous factors. In order to understand the large-scale recording capabilities and potential limitations of multisite probes, it is important to quantify this variability, and to determine whether certain key device parameters influence the recordings. Here we investigate the effect of four parameters, namely, electrode surface, width of the structural support shafts, shaft number, and position of the recording site relative to the shaft tip. This study employs acutely implanted silicon probes containing up to 64 recording sites, whose performance is evaluated by the metrics of noise, spike amplitude, and spike detection probability. On average, we find no significant effect of device geometry on spike amplitude and detection probability but we find significant differences among individual experiments, with the likelihood of detecting spikes varying by a factor of approximately three across trials.

Keywords

silicon neural probes; multielectrode arrays; MEMS

1. Introduction

Micro and nanofabricated electrode arrays enable extracellular electrical measurements from multiple neurons in parallel (Stevenson and Kording, 2011; Wise et al., 2008), offering the prospect of observing more comprehensive patterns of neuronal network activity underlying behavior, emotion, and cognition. However, scaling up the number of sites on an electrode array does not guarantee extracellular action potentials (EAPs or spikes) from more putative units. In conventional single-electrode measurements, the electrode depth may be fine-tuned

*Corresponding author: smasmanidis@ucla.edu.
[3]Present address: Department of Brain and Cognitive Sciences, Massachusetts Institute of Technology, Cambridge, USA.
[4]Present address: Department of Neurobiology, David Geffen School of Medicine, University of California, Los Angeles, USA.

to maximize EAP amplitude, thereby improving single-unit classification (Fee and Leonardo, 2001). However, this strategy does not appear as effective in multisite planar silicon probe experiments in which all sites move concurrently, as improving the signal on one channel may accompany signal deterioration at another nearby channel. Multisite silicon probes offer the prospect of recording from large neuronal populations relatively free of selection bias; on the other hand the EAP amplitude, which directly impacts the ability to isolate single-units, is expected to vary significantly between experiments. Before embarking on efforts to further scale up the recording capabilities of micro and nanofabricated probes, here we quantify this variability for a set of devices, and investigate the effect of some key device design parameters on EAP amplitude.

The ensemble of extracellular spikes from a neural probe inserted in the brain will depend on the electrodes' location relative to surrounding neurons. No two device insertions will produce identical spike amplitude recording conditions, but it is possible that some neural interfaces are more suitable than others at yielding high quality measurements. Despite an abundance of micromachined neural probes based on silicon and other substrates (Cheung, 2007), a thorough analysis of their recording performance as a function of device parameters such as shaft size has not been carried out. Nevertheless, such probes present an ideal platform with which to systematically explore these issues. The goal of this work is to provide insight into the following questions: (i) which device parameters improve EAP amplitude or reduce noise; (ii) in a given experiment, what is the likelihood of measuring action potentials on a randomly selected recording site; and (iii) what are the dominant factors that contribute to variability in recording quality across multiple experiments?

We speculate that EAP amplitude indirectly reflects the amount of damage inflicted by an implanted device on neurons in its vicinity. This hypothesis is based on the rapid spatial attenuation of EAP strength with increasing distance from the soma (Gold et al., 2006; Gray et al., 1995), implying that high-amplitude spike events most likely originate from neurons in the immediate vicinity of the electrode (50–100 μm). Furthermore, the hypothesis assumes that cell bodies closest to the probe are most likely to sustain injury during insertion and thus not appear in a measurement (Blanche et al., 2005). If this assumption is valid, then it is expected that on average, the wider the damaged perimeter of neurons surrounding the probe shaft, the fewer high-amplitude spikes will appear in a measurement.

An estimation of how many neurons should lie within the `listening range' of a microelectrode, based on cell density and known properties of extracellular fields and noise, predicts tens to hundreds of neurons per channel (Buzsaki, 2004). However, the actual number is usually one to two orders of magnitude less than predicted – in the single digits, or zero (Shoham et al., 2006). Given that the typical number of recorded units is much lower than might be expected, we ask whether certain parameters of the recording device, such as its size, influence the measurements, and also how much variation in yield is expected between trials.

A wide range of device parameters may affect recording performance because of tissue damage (Bjornsson et al., 2006) and other amplitude-limiting effects. Here we focus our investigation to four key parameters on EAP amplitude: (i) recording site gold plating to reduce impedance, (ii) shaft width, (iii) the number of shafts, and (iv) the position of the site on the array. To account for trial-to-trial variability in our results, we obtained electrophysiological measurements from multiple animals and recording depths in the brain. Silicon-based probes employing up to 64 recording sites were repeatedly inserted in the CA1 and CA3 regions and the dentate gyrus (DG) of the mouse hippocampus. These areas were selected for their relatively homogeneous concentration of pyramidal or granule neurons at discrete depths, which could be reliably targeted with stereotaxic techniques.

Previous studies on planar silicon-based neural probe performance have examined changes in EAP quality over chronic timescales of days to months (Vetter et al., 2004; Ward et al., 2009). However, it has been unclear whether the geometrical specifications of the silicon shafts as well as electrode impedance influence EAP measurements on acute timescales. Here, we address this issue by conducting measurements with implanted interfaces over timescales of minutes to hours following device insertion.

2. Methods

2.1 Recording system design and operation

Figure 1 illustrates the two microelectrode array designs employed in these experiments, which are subsequently referred to as the `4×16' and `1×64' structures. Their fabrication process has been described previously (Du et al., 2011). Both probes contain 64 108-μm^2 gold recording sites, arranged in single rows on the 4×16 structure and in three staggered rows with at least 35 μm between electrode centers on the 1×64 structure. Silicon shafts are 23 μm thick, and their width is tapered from 28–40 and from 60–85 μm for the 4×16 and 1×64 structures, respectively. The shafts of the 4×16 structure are separated by 250 μm.

Electrophysiological signals on the probe were read out via an application-specific integrated circuit (ASIC) enabling wide band (1–6,400 Hz) multiplexed data acquisition with a sampling rate of 22,300 Hz per channel (Du et al., 2011). Analog multiplexed signals were digitized with 16 bit resolution (USB-6251, National Instruments, Austin TX) and stored for offline analysis. The ASIC was also used to measure electrode impedance at 1 kHz, and to electrodeposit gold in order to modify electrode impedance, as described in Du *et al.*, 2011. The electrodeposited gold protruded 1–4 μm from the planar probe surface. Impedance was determined via a two-terminal measurement between the test electrode and a macroscopic platinum reference electrode, with a 1 nA input current. Gold plating was carried out by applying −1.5 V relative to a platinum reference wire in gold plating solution (Sifco, Cleveland OH). Electrodes whose impedance could not be reduced below 3 MΩ post-plating were considered non-functional and excluded from further analysis. The 4×16 device contained one non-functional site; the two 1×64 devices used here had three and seven non-functional sites, respectively. All data acquisition, electroplating and impedance testing functions were carried out with custom-written LabVIEW code (National Instruments, Austin TX). Offline analysis was conducted using Matlab (The Mathworks, Natick MA). Data were digitally bandpass filtered in the spike frequency band from 300–6000 Hz via a 3rd order Butterworth filter. All recordings were performed with the reference electrode connected to the ground terminal.

2.2 Acute in vivo measurements

All surgical procedures were approved by the Caltech IACUC. 25–30 g male C57BL/6J mice were anesthetized with chloral hydrate (400 mg/kg, i.p.), and placed in a stereotaxic frame apparatus (Kopf Instruments, Tujunga CA). Body temperature was regulated with a heating pad. The depth of anesthesia was regularly checked, and additional anesthetic dose was given as necessary. After reflecting skin on the scalp, one to four ~0.5 mm^2 craniotomies were made with a drill over the hippocampal formation (1.75±0.5 mm AP and 1.5±0.5 mm ML relative to bregma), taking care to not rupture the dura. A slit was made in the dura with a syringe needle to allow passage of the silicon probe. The recording system was mounted on a motorized micromanipulator (MP-225, Sutter Instruments, Novato CA). The orientation of the rod used to hold the probe onto the micromanipulator arm could be fine-tuned via an adjustable stage (Kinematic Mirror Mount, Thor Labs, Newton NJ). This allowed precise alignment of the probe shaft to within ±0.4° of the axis of motion, helping to ensure virtually identical insertion conditions across different animals and penetrations, and

to minimize insertion-related tissue damage (Edell et al., 1992). After alignment, the probe was lowered into the brain at a speed of ≤10 μm/s under the control of the motorized micromanipulator. We did not observe any sign of probe bending during insertion.

In order to provide each site on the array the opportunity to land in the CA1, CA3 and dentate gyrus cell body layers in the hippocampus, experiments involved alternately recording blocks of data and advancing the probe in increments of 50–100 μm, corresponding to the approximate thickness of the cell body layers. After adjusting the probe depth, we allowed at least 100 s for tissue to settle before initiating the data acquisition. Thus each device penetration generated multiple recording blocks. To maximize the number of blocks and penetrations per animal, the block duration was set to 200 s. We computed the depth of each recording site from its position relative to the probe tip, and the tip's position relative to bregma on the skull. Only recordings at site depths of 1 to 3 mm, encompassing the dorsoventral extent of the hippocampus, were included in further analysis. We analyzed a total of 20 penetrations from 11 mice. Different insertion locations in the same animal were separated by at least 0.5 mm.

An Ag/AgCl ground electrode wire, which also served as the amplifier reference electrode, was placed in a saline bath on the exposed craniotomy. Probes were reused after cleaning them between experiments in trypsin (Invitrogen, Grand Island NY) for 20 min and rinsing with deionized water. In previous work we reported a gradual increase in the electrode impedance following repeated penetrations (Du et al., 2011), which we attribute to partial detachment of electrodeposited gold during insertion. In order to minimize variability in electrode surface quality between experiments, at the conclusion of each recording session we measured impedance and redeposited gold if the mean impedance across all functional sites exceeded 1 MΩ. Re-plating was usually performed after four penetrations. Under these device maintenance conditions we did not observe accumulation of any debris on the silicon shafts or electrodes, or evidence for any other form of physical damage after dozens of recording sessions. Furthermore, we did not find significant differences in EAP amplitude recorded on freshly plated versus old plated electrodes. At the conclusion of a recording session, animals were overdosed with ketamine/xylazine and transcardially perfused. Brain slices were obtained to verify passage of the probe through the targeted zones of the hippocampus.

2.3 Selection of recording quality metrics

We defined the noise level as the 68^{th} percentile of the absolute value of the filtered data from a recording block. This corresponds to the standard deviation (root-mean-square) of the signal for Gaussian noise, but is insensitive to the presence of action potentials without requiring explicit spike detection. To identify putative EAP or spike-like noise events, we detected all the local voltage minima in a block, in 1 ms windows, and extracted their waveforms. In evaluating probe performance, we avoided spike sorting techniques in order to minimize the use of subjective spike classification criteria. Instead, we employed straightforward performance metrics which provide information on the largest observed EAPs, which are the signals thought most likely to be affected by cellular damage and other sources of variation. The `signal' was defined as the mean negative peak amplitude of the 10 largest spike-like events per 200 s block on a given recording site. Although we did not explicitly require these 10 events to correspond to the same single unit, in most cases we observed that they exhibited a similar characteristic waveform, suggesting they originate from the same unit. Our results were qualitatively similar for signal definitions using 2 to 100 spikes per 200 s block. We did not attempt to categorize putative signals based on extracellular waveform width, which has been reported to reflect pyramidal or interneuron action potentials (Bartho et al., 2004).

Note that the above definition of signal does not rely on setting an amplitude threshold, and thus makes no distinction between high and low-amplitude EAPs or non-neuronal spike-like fluctuations. For instance, in measurements that were carried out in saline solution, the mean recorded `signal' was 15 μV and the maximum was 35 μV. To discriminate between these noise-related events and putative EAPs, we designated `spikes' as signals exceeding a threshold of 70 μV in negative peak amplitude. This value corresponds to moderately high amplitude EAPs, however, this criterion does not imply that smaller amplitude signals could not be reliably detected or sorted, and in fact, we routinely measured ~50 μV putative EAPs. In accordance with this threshold, the `spike yield' denotes the fraction of 200 s recording blocks from a selected set of channels and/or locations in the brain which display spikes. The yield measures the probability of detecting spikes (signal measurements >70 μV) across a group of recordings.

2.4 Statistical analysis

Nonparametric analysis was used wherever possible to compare sets of measurements. We used the Mann-Whitney U-test and its extension to three or more groups, the Kruskal-Wallis (KW) test, to check for differences in population medians against a null hypothesis that all distributions sampled have equal medians. In demonstrating similar spike amplitude populations, we used the more stringent Kolmogorov-Smirnov (KS) test, with a null hypothesis that populations were sampled from the same continuous distribution.

Because several parameters other than probe type could affect signal measurements, we used ANOVA to compare the various device geometries while allowing random effects of penetration index, site depth within a penetration, recording number, channel number, and (in the case of the 4×16 devices) shaft number. To account for possible measurement bias arising from the longer arrays (1×64) accessing a greater depth range in the brain than the shorter arrays (1×16 and 4×16), in comparing device geometries we only included channels within 0.62 mm of the electrode nearest the tip. Although the complete sets of measurements are not distributed normally, we expected that the few measurements within individual blocks—e.g. from the same recording site and depth within a particular penetration—were sampled independently from normal distributions, thus satisfying the formal requirements of ANOVA.

To compare sources of variation within the 1×64 recordings, and to test for variation in recording quality based on position on the array, we performed ANOVA on the signal, noise, and spike amplitude measurements from the 1×64 probe. We included random effects of (i) recording block, (ii) recording site, (iii) penetration index, and (iv) recording site position (i.e., depth during a particular penetration), as well as fixed effects of (v) site position along the longitudinal axis (in four groups spanning from the tip to base) and (vi) medial-lateral site position (center or edge).

2.5 Stability of recording in one location over acute timescales

In experiments with silicon probes it is common practice to allow tissue around the inserted devices to settle for up to an hour before acquiring data (Niell and Stryker, 2008). It is not known whether our relatively short settling time (100 s) and recording block duration (200 s) might lead to erroneous conclusions about the recording performance of a probe, i.e., whether the performance markedly improves on the timescale of an hour. Hence we evaluated the stability of recordings using a 1×64 probe by continuously acquiring data for one hour at a single position encompassing the hippocampal formation. The mean noise level across channels remained between 5 and 10 μV for the duration of the recording. Signal values on individual channels were also relatively stable, with a mean standard deviation per channel of 6 μV, which is considerably less than our threshold for detecting

spikes. Representative curves are shown in Fig. 2a. The ten waveforms per 200 s used to compute the signal values remained qualitatively similar on each channel throughout the recording (see example inlays in Fig. 2b). Given that signals appear stable over the timescale of one hour, we used 200 s recording blocks without concern that spike amplitudes would appreciably vary (e.g., from units appearing or disappearing because of probe-tissue micromotion effects). However, notwithstanding the time constraints imposed by our experiments, allowing long settling times may minimize signal drift, and thus allow more reliable single-unit isolation.

3. Results

3.1 High-amplitude signals recorded at characteristic locations in the brain

Recordings were conducted in 200 s blocks at a series of depths as the probe was gradually advanced into the brain. When signal values were plotted as a function of site depth, we found two distinct regions of high amplitude activity (Fig. 3a). Such regions occurred at approximately 1.4 and 2.2 mm depth, and based on our analysis of probe track locations in brain sections, these areas correspond to the CA1, as well as either the CA3 or DG cell body layers of the hippocampus (Fig. 3b). When recordings were repeated during gradual extraction of the probe, large spikes were observed at the same site depths as during the descent. This confirms that these regions of high activity correspond to distinct anatomical formations in the brain, and suggests that variation in the position of high-activity regions was due to experimental differences in probe trajectories taken during each penetration. Henceforth we only discuss measurements made during the descending phase of the experiments.

In each penetration we reliably observed both localized regions of high and low spike yield. We observed a maximum spike yield of 54 to 100% (median 87%) within 100 μm regions of the brain, which likely corresponded with the pyramidal cell layers of the CA1 or CA3 regions or the granule cell layer of the DG. It is striking that despite finding ~100 μm regions along the insertion track with up to 100 % spike yield, we also observed extended regions (~500 μm) containing no spikes. The low firing rate in these regions, which coincide with the stratum radiatum or stratum lacunosum-moleculare, reflects both significantly lower cell body density in these intermediate layers of the hippocampus, and possibly also anesthesia-related suppression of neuronal firing.

3.2 Electroplating reduces noise but does not affect spike amplitude

The deposition of electrically conducting materials such as metals, polymers or carbon nanotubes onto the electrode surface provides a means of improving the performance of neural recording interfaces (Kotov et al., 2009). However, it has not been systematically studied whether the addition of electrode surface area in the form of electrodeposited gold might attenuate extracellular action potentials. Such signal attenuation effects have been modeled as a function of electrode geometric area (Lempka et al., 2011; Moffitt and McIntyre, 2005), but the dependence on surface area is less apparent. This issue is important in light of the growing use of various deposition techniques to modify the electrode surface (Cui et al., 2001).

Our 64 site probes and accompanying recording systems are well suited to elucidating this issue, as they enable multiple measurements in parallel, and the electrodes are readily amenable to impedance measurements and electroplating. Moreover, the low noise level (~2 μV) of the electronic amplifiers (Harrison, 2008) allows variations in other sources of noise, such as fluctuations at the electrode-fluid interface to be discerned (Du et al., 2011). To assess the impact of electroplating on recordings with the silicon probes, we compared both

signal and noise from measurements using an unplated 4×16 probe, to measurements using the same probe containing freshly electrodeposited gold. The mean impedance at 1 kHz across the array was 3.8 and 0.4 MΩ pre and post-plating, respectively. Figure 4a displays the mean noise level of all measured electrodes (n=63). As expected, we found a reduction in noise associated with gold plating both in saline and *in vivo* ($p<0.001$, U-test), presumably because the increased effective surface area decreases electrode impedance. As Fig. 4a illustrates, the average noise level fell from 7.2 to 5.6 μV *in vivo* and from 5.6 to 2.2 μV in saline after electrodes were plated, consistent with the effects of impedance on saline noise measurements discussed in Du et al. (2011).

In contrast to the decrease in noise level with plating, we observed an insignificant increase in median spike amplitude ($p>0.1$, U-test), and a slight increase in the fraction of recording sites displaying spikes exceeding 70 μV (from 14 to 20%). The signal probability distributions from the unplated and plated probes are plotted in Fig. 4b. The results show that gold-plating improves SNR via noise reduction with no apparent detrimental effect on EAP amplitude, thereby facilitating detection of spikes. For all subsequent tests the probes were gold-plated before collecting data.

3.3 Minimal impact of shaft width and number on spike amplitude

Next, we investigated whether the physical dimensions of silicon probes affects recordings in acute experiments, focusing on two geometric parameters: the width of the shaft, and the number of shafts. We explored whether probes with larger cross section, or more than one shaft induce a wider perimeter of damaged neurons, which would be manifested as lower average EAP amplitude. To evaluate the effect of cross-section, we compared single-shaft devices (one 1×16 device and two 1×64 devices), which had widths of 28–40, and 60–85 μm, respectively. To evaluate the effect of shaft number, we compared a 4×16 probe, which contains four shafts spaced by 250 μm, to a 1×16 structure. In order to avoid other possible sources of variation in the devices at the level of microscopic differences arising during fabrication, the 1×16 device was produced by breaking three of the four shafts from the 4×16 probe. These effects were unavoidable in comparing the 1×16 to the 1×64 device, but we believe that the populations of recording sites sampled are sufficiently representative given the variation across channels and across penetrations to demonstrate comparable performance of the two geometries. Using ANOVA (see Section 2.4) we observed no significant effect ($p > 0.4$) of shaft width or shaft number on signal measurements.

Additionally, we directly examined the populations of measured spike amplitudes from each of the three device geometries (Fig. 5a). Strikingly, there was no difference between the spike amplitude distributions observed with the 1×16 probe and the corresponding shaft on the original unbroken 4×16 probe ($p=0.3$, KS test), even though a significant difference could arise simply from differences among the penetrations performed by the two probes. The widest (1×64) probe, which might be expected to induce the thickest perimeter of damaged neurons, indeed yielded the smallest median spike amplitude (102 μV versus 109 μV for the next lowest value from shaft A on the 4×16 probe). However, the distribution of spike amplitudes on the 1×16 probe was statistically indistinguishable from shaft A on the 4×16 device ($p=0.4$, KS test), again despite potential variation across penetrations.

We also assessed recording performance by comparing penetration-wise spike yields of the three device types (Fig. 5b), and found no significant difference ($p=0.9$, KW test). The fraction of recordings during a given penetration which had spikes was ~21±1% (s.e.m.), averaged across penetrations using all probe geometries discussed in this study and including from each penetration recordings from areas of both high and low cell density in the hippocampus.

3.4 Sources and magnitude of variation in extracellular recordings

Trial-to-trial variation in the observed noise, spike amplitude, and spike detection probability are an intrinsic property of recordings with multisite silicon probes, but the magnitude of this variation has not been analyzed in detail. To explore this issue, we used ANOVA (see section 2.4) to quantify the variability in recordings from a single device architecture (the 1×64 variant), which contains 64 electrodes arranged in a three staggered row pattern spanning 1.31 mm.

We first compared the relative contribution of what we speculated to be the four main sources of variation in noise and signal amplitude: (i) recording block, (ii) recording site, (iii) penetration index, and (iv) recording site position (i.e., depth during a particular penetration). Normalized variance components explained by each of the above factors are shown in Fig. 6a, with Figs. 6b and 6c displaying histograms of the corresponding noise and signal amplitude measurements. Any variations which could not be systematically accounted for by these effects were designated as `other', presumably random mechanisms we believe are related to the inconsistent spacing between a recording site and the nearest active neuron. We find that noise depends strongly on the specific recording block and channel number, and weakly on the actual site location along the depth of the hippocampus. This result might arise from either gradual accumulation of electrically resistive tissue on the electrodes, or removal of electrodeposited gold as the probe is advanced in the brain; either of these effects would increase impedance and therefore progressively elevate noise. It is worth noting that inter-regional differences in noise have been measured, implying that noise in the hippocampus may not be representative of all other brain structures (Buchwald and Grover, 1970). In contrast to noise, the source of variability in signal and spikes is primarily accounted for by undefined, presumably random mechanisms (e.g., how close the site is to a particular neuron) and secondly by approximate recording site location in the hippocampus, but not by the recording block or specific channel.

Next we tested for systematic variations in recording quality as a function of site position on the array, searching whether certain regions of the 1×64 electrode array, such as the tip, or edges, were more favorably situated to record high-amplitude EAPs. There was no significant effect of longitudinal or medial-lateral recording site position on the array ($p>0.2$) on the amplitude of observed spikes (Fig. 7a). For example, EAPs >300 μV were observed from all regions of the electrode array. Furthermore, there was <10% variation among the median spike amplitudes observed across the longitudinal channel groups, and only 1% between the center and edge channels.

Although we found no significant effect of site position on the array with these probes, there was evidently substantial trial-to-trial variability. We therefore sought to characterize typical spike yield variation across several penetrations. Figure 7b indicates the observed spike yields grouped by channel and by penetration. The channel-wise spike yield varied with an interquartile range of 15 to 28%. That is, the likelihood of detecting spikes on a particular site as a probe was lowered into the hippocampus varied about twofold across all sites. Similarly, penetration-wise spike yield ranges by almost threefold, from 12 to 32%, over the nine penetrations performed for these experiments.

4. Discussion

We have investigated the effect of some important device parameters, pertaining to electrode impedance and geometry, on acute action potential measurements in the mouse hippocampus. Though it has long been known that the signals recorded with multisite electrodes vary between experiments, even within the same brain areas, to the authors' knowledge this is the first report to systematically characterize this variability. The

hippocampus served as the test site for neural probe performance evaluation, which has often been the case thanks to its dense, easily identifiable cell body layers and interesting functional properties (Csicsvari et al., 2003; Henze et al., 2000). Our conclusions are summarized and interpreted as follows.

First, we confirmed once again that electroplating of electrodes reduces noise, but also demonstrated the increased conducting surface area does not affect spike amplitude. Thus electroplating is an effective approach to improving signal-to-noise ratio, and is presumably useful for both acute and chronically implanted neural interfaces (Ludwig et al., 2011). These results also underscore that recorded extracellular signals, and noise, are largely determined by different mechanisms, although the single largest source of noise was not due to intrinsic electrode properties, but rather the background neuronal activity from distant active neurons (`neural hash', Fig. 4a).

Thus strategies to improve the signal-to-noise ratio can either focus on noise reduction via electroplating and low-noise instrumentation, or signal enhancement, which is more challenging, but could entail interventions to induce neurons to migrate or grow closer to the probe (Purcell et al., 2009). In light of these different SNR-determining mechanisms, it may be insightful to report both signal and noise when assessing various aspects of neural interface performance.

Second, we found no significant difference in spike amplitude between devices containing a single 40 μm wide shaft, or four 40 μm shafts separated by 250 μm. Nor was a difference in amplitude measurements found between the 40 and 85 μm wide device, although we do not have positive proof that the 85 μm wide probe was able to record spikes larger than ~600 μV, which were occasionally observed with its narrower counterpart (Fig. 5a). It therefore appears that multiple shafts spaced ≥250 μm apart, or shafts ≤85 μm wide, do not significantly diminish the EAP amplitude in acute measurements relative to a single 40 μm wide shaft. A smaller implant is obviously preferable as it will interfere less with the blood-brain barrier (Kozai et al., 2010; Mitala et al., 2008) and neuronal processes (Claverol-Tinture and Nadasdy, 2004), both of which may have a rapid disruptive effect on recorded cells' functionality. However, the above results indicate that for acutely implanted probes, the quality of recordings in mice is independent of probe cross section at least as high as 85×23 μm^2. Whether this result applies to larger or more closely spaced silicon microstructures, or different species, remains an open question for future investigations. Silicon probes at least as wide as 212 μm have been successfully used to record multiple single-units (Blanche et al., 2005), although owing to differences in silicon shaft thickness and recording site geometry and composition, a systematic performance comparison with the devices presented here could not be carried out. Interestingly, histological studies of chronically implanted probes report that a larger device cross-section leads to a larger volume of inflammation (Seymour and Kipke, 2007; Stice et al., 2007; Thelin et al., 2011). Based on those observations, we might expect to observe size-dependent deterioration in EAPs on the timescale of a few weeks, which coincides with the progression of brain's inflammatory response to implanted microdevices (Turner et al., 1999). However, another study indicates that device size effects may come more into play in the short term, but in the long term the inflammatory response is size-independent (Szarowski et al., 2003). Hence, although we speculate that a small device cross-section may be critical for chronically maintaining neural interface stability, a clear understanding of the relationship between size, inflammatory response, and chronic electrophysiological recording performance has yet to emerge. Nevertheless, the characterization in this paper contributes to the foundation for detailed *in vivo* analysis of neuronal circuits via high-density multielectrode recordings. Numerous contemporary applications of high-density multielectrode recordings can be

performed in the acute situation, bypassing the pitfalls associated with chronically implanted electrodes (Goard and Dan, 2009; Niell and Stryker, 2010).

Third, the location of the recording site on the electrode array does not influence EAP amplitude; pad electrodes at the tip or the edge of the probe are as effective at measuring spikes as those at the base or center. These results were obtained from an array spanning 1.3 mm tip-to-base, suggesting that EAP amplitude is unaffected across at least that length scale. We do not find evidence for more damage in the form of smaller spikes on the base of the probe (after the tip has passed through a particular region), or smaller spikes when the probe is extracted. The finding that basal sites measure as effectively as sites at the tip may depend on the ability to align the probe such that it points precisely in the direction of insertion (Edell et al., 1992). These results also suggest that electrode arrays spanning greater lengths may be feasible, and thus work on further enhancing the recording site density and number on silicon-based probes is worthwhile (Ruther et al., 2010).

Finally, we find substantial variability in the yield of detected spikes between each penetration even if all trials target nearly identical stereotaxically defined anatomical regions, with performance varying almost threefold, from 12 to 32%. Although we did not explicitly analyze single-units, our results predict that the number of isolated units will vary by a similar amount on a trial-to-trial basis. Discrepancies in yield presumably arise via microscale differences in the path taken by the recording array near neurons, which can result in considerable deviations in EAP amplitude. On the other hand, the bimodal shape of the activity profile shown in Fig. 3 is a reliably measured feature in our recordings, although the exact depth of the peaks varies from trial to trial. Despite this significant variation in large-scale extracellular measurements, the mean spike detection yield per penetration provides a useful benchmark; on average, as a probe is moved through the hippocampus, we expect a randomly chosen recording channel to have a ~20% probability of registering spikes >70 μV (averaged across regions of low neuronal density, such as stratum radiatum and lacunosum-moleculare, and regions of high activity such as CA1, CA3, and DG cell body layers where nearly 100% of the channels may record spikes).

In a typical single- or few-electrode recording experiment, the experimenter may adjust the position of the probe to seek out prominent spikes; but the most prominent spikes may represent only a subset of active or functionally interesting neuronal subpopulations. The dense and distributed spatial sampling capabilities of multisite silicon-based arrays minimizes such distortions.

Acknowledgments

We thank T. J. Blanche for discussions on probe design and recording quality assessment, R. R. Harrison for developing the ASIC used to read out data from the probe, and M. L. Roukes for device fabrication support. Neural probe nanofabrication was carried out at the Kavli Nanoscience Institute at Caltech, and the Nanoelectronics Research Facility at UCLA. We acknowledge support from the Broad Foundations, the Della Martin Fund for Discoveries in Mental Illness, and the NIH (DA-17279, AG-033954).

References

Bartho P, Hirase H, Monconduit L, Zugaro M, Harris KD, Buzsaki G. Characterization of neocortical principal cells and Interneurons by network interactions and extracellular features. Journal of Neurophysiology. 2004; 92:600–8. [PubMed: 15056678]

Bjornsson CS, Oh SJ, Al-Kofahi YA, Lim YJ, Smith KL, Turner JN, De S, Roysam B, Shain W, Kim SJ. Effects of insertion conditions on tissue strain and vascular damage during neuroprosthetic device insertion. Journal of Neural Engineering. 2006; 3:196–207. [PubMed: 16921203]

Blanche TJ, Spacek MA, Hetke JF, Swindale NV. Polytrodes: high-density silicon electrode arrays for large-scale multiunit recording. J Neurophysiol. 2005; 93:2987–3000. [PubMed: 15548620]

Buchwald JS, Grover FS. Amplitudes of background fast activity characteristic of specific brain sites. J Neurophysiol. 1970; 33:148–59. [PubMed: 5411510]

Buzsaki G. Large-scale recording of neuronal ensembles. Nature Neuroscience. 2004; 7:446–51.

Cheung KC. Implantable microscale neural interfaces. Biomed Microdevices. 2007; 9:923–38. [PubMed: 17252207]

Claverol-Tinture E, Nadasdy Z. Intersection of microwire electrodes with proximal CA1 stratum-pyramidale neurons at insertion for multiunit recordings predicted by a 3-D computer model. Ieee T Bio-Med Eng. 2004; 51:2211–6.

Csicsvari J, Henze DA, Jamieson B, Harris KD, Sirota A, Bartho P, Wise KD, Buzsaki G. Massively parallel recording of unit and local field potentials with silicon-based electrodes. Journal of Neurophysiology. 2003; 90:1314–23. [PubMed: 12904510]

Cui X, Lee VA, Raphael Y, Wiler JA, Hetke JF, Anderson DJ, Martin DC. Surface modification of neural recording electrodes with conducting polymer/biomolecule blends. J Biomed Mater Res. 2001; 56:261–72. [PubMed: 11340598]

Du J, Blanche TJ, Harrison RR, Lester HA, Masmanidis SC. Multiplexed, high density electrophysiology with nanofabricated neural probes. PLoS One. 2011; 6:e26204. [PubMed: 22022568]

Edell DJ, Toi VV, Mcneil VM, Clark LD. Factors Influencing the Biocompatibility of Insertable Silicon Microshafts in Cerebral-Cortex. Ieee T Bio-Med Eng. 1992; 39:635–43.

Fee MS, Leonardo A. Miniature motorized microdrive and commutator system for chronic neural recording in small animals. J Neurosci Methods. 2001; 112:83–94. [PubMed: 11716944]

Goard M, Dan Y. Basal forebrain activation enhances cortical coding of natural scenes. Nature Neuroscience. 2009; 12:1444–9.

Gold C, Henze DA, Koch C, Buzsaki G. On the origin of the extracellular action potential waveform: A modeling study. J Neurophysiol. 2006; 95:3113–28. [PubMed: 16467426]

Gray CM, Maldonado PE, Wilson M, McNaughton B. Tetrodes markedly improve the reliability and yield of multiple single-unit isolation from multi-unit recordings in cat striate cortex. J Neurosci Methods. 1995; 63:43–54. [PubMed: 8788047]

Harrison RR. The design of integrated circuits to observe brain activity. P Ieee. 2008; 96:1203–16.

Henze DA, Borhegyi Z, Csicsvari J, Mamiya A, Harris KD, Buzsaki G. Intracellular features predicted by extracellular recordings in the hippocampus in vivo. Journal of Neurophysiology. 2000; 84:390–400. [PubMed: 10899213]

Kotov NA, Winter JO, Clements IP, Jan E, Timko BP, Campidelli S, Pathak S, Mazzatenta A, Lieber CM, Prato M, Bellamkonda RV, Silva GA, Kam NWS, Patolsky F, Ballerini L. Nanomaterials for Neural Interfaces. Adv Mater. 2009; 21:3970–4004.

Kozai TDY, Marzullo TC, Hooi F, Langhals NB, Majewska AK, Brown EB, Kipke DR. Reduction of neurovascular damage resulting from microelectrode insertion into the cerebral cortex using in vivo two-photon mapping. Journal of Neural Engineering. 2010; 7

Lempka SF, Johnson MD, Moffitt MA, Otto KJ, Kipke DR, McIntyre CC. Theoretical analysis of intracortical microelectrode recordings. J Neural Eng. 2011; 8:045006. [PubMed: 21775783]

Ludwig KA, Langhals NB, Joseph MD, Richardson-Burns SM, Hendricks JL, Kipke DR. Poly(3,4-ethylenedioxythiophene) (PEDOT) polymer coatings facilitate smaller neural recording electrodes. J Neural Eng. 2011; 8:014001. [PubMed: 21245527]

Mitala CM, Wang YX, Borland LM, Jung M, Shand S, Watkins S, Weber SG, Michael AC. Impact of microdialysis probes on vasculature and dopamine in the rat striatum: A combined fluorescence and voltammetric study. J Neurosci Meth. 2008; 174:177–85.

Moffitt MA, McIntyre CC. Model-based analysis of cortical recording with silicon microelectrodes. Clin Neurophysiol. 2005; 116:2240–50. [PubMed: 16055377]

Niell CM, Stryker MP. Highly selective receptive fields in mouse visual cortex. J Neurosci. 2008; 28:7520–36. [PubMed: 18650330]

Niell CM, Stryker MP. Modulation of Visual Responses by Behavioral State in Mouse Visual Cortex. Neuron. 2010; 65:472–9. [PubMed: 20188652]

Purcell EK, Seymour JP, Yandamuri S, Kipke DR. In vivo evaluation of a neural stem cell-seeded prosthesis. Journal of Neural Engineering. 2009; 6

Ruther P, Herwik S, Kisban S, Seidl K, Paul O. Recent Progress in Neural Probes Using Silicon MEMS Technology. Ieej T Electr Electr. 2010; 5:505–15.

Seymour JP, Kipke DR. Neural probe design for reduced tissue encapsulation in CNS. Biomaterials. 2007; 28:3594–607. [PubMed: 17517431]

Shoham S, O'Connor DH, Segev R. How silent is the brain: is there a “dark matter” problem in neuroscience? Journal of Comparative Physiology a-Neuroethology Sensory Neural and Behavioral Physiology. 2006; 192:777–84.

Stevenson IH, Kording KP. How advances in neural recording affect data analysis. Nature Neuroscience. 2011; 14:139–42.

Stice P, Gilletti A, Panitch A, Muthuswamy J. Thin microelectrodes reduce GFAP expression in the implant site in rodent somatosensory cortex. Journal of Neural Engineering. 2007; 4:42–53. [PubMed: 17409479]

Szarowski DH, Andersen MD, Retterer S, Spence AJ, Isaacson M, Craighead HG, Turner JN, Shain W. Brain responses to micro-machined silicon devices. Brain Research. 2003; 983:23–35. [PubMed: 12914963]

Thelin J, Jorntell H, Psouni E, Garwicz M, Schouenborg J, Danielsen N, Linsmeier CE. Implant size and fixation mode strongly influence tissue reactions in the CNS. Plos One. 2011; 6:e16267. [PubMed: 21298109]

Turner JN, Shain W, Szarowski DH, Andersen M, Martins S, Isaacson M, Craighead H. Cerebral astrocyte response to micromachined silicon implants. Exp Neurol. 1999; 156:33–49. [PubMed: 10192775]

Vetter RJ, Williams JC, Hetke JF, Nunamaker EA, Kipke DR. Chronic neural recording using silicon-substrate microelectrode arrays implanted in cerebral cortex. Ieee T Bio-Med Eng. 2004; 51:896–904.

Ward MP, Rajdev P, Ellison C, Irazoqui PP. Toward a comparison of microelectrodes for acute and chronic recordings. Brain Res. 2009; 1282:183–200. [PubMed: 19486899]

Wise KD, Sodagar AM, Yao Y, Gulari MN, Perlin GE, Najafi K. Microelectrodes, microelectronics, and implantable neural microsystems. P Ieee. 2008; 96:1184–202.

- We characterized the recording performance of multisite silicon probes.
- We characterized performance in terms of noise, extracellular action potential amplitude, and detection probability.
- We found trial-to-trial variability of a factor of three in the probability of detecting spikes.

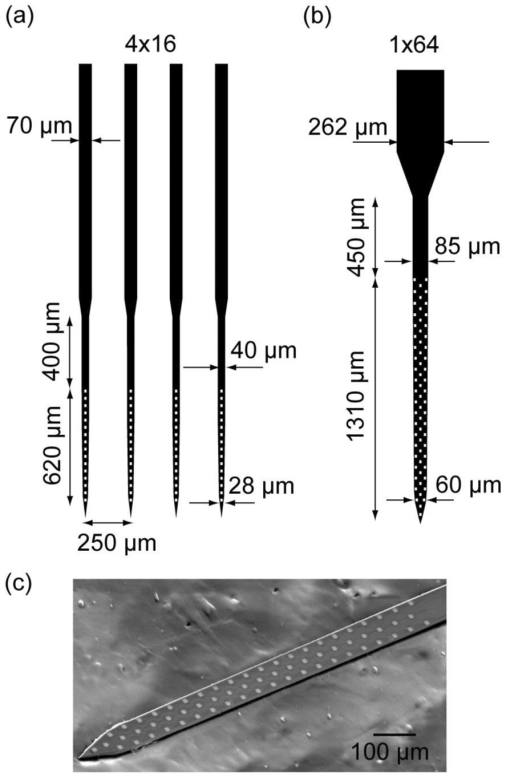

Fig. 1.

64 channel neural probes used to assess recording variability. (a) The `4×16' device with four 40 µm wide shafts. On each shaft, 16 recording sites with an area of 108 $\mu m^2$ (white rectangles) are aligned in a single row extending 620 µm. Adjacent shafts are 250 µm apart. (b) The `1×64' device with a single 85 µm-wide shaft. The recording sites are distributed in a three staggered row pattern, extending 1310 µm from the tip. (c) Scanning electron microscope image of a 1×64 probe.

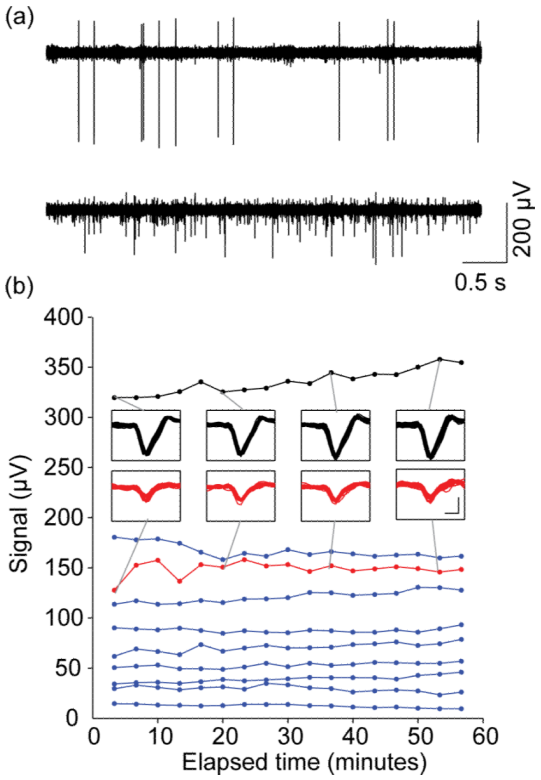

Fig. 2.

Recording quality does not change appreciably over one hour. (a) Recording segments from two sites on a 1×64 probe. (b) Representative signal values over one hour of recording. Each trace represents one electrode input channel, and each signal measurement is computed using 200 s of data. Insets show the ten spike-like events used to compute the signal for the two channels shown in (a). Scale bars denote 0.2 ms and 200 µV.

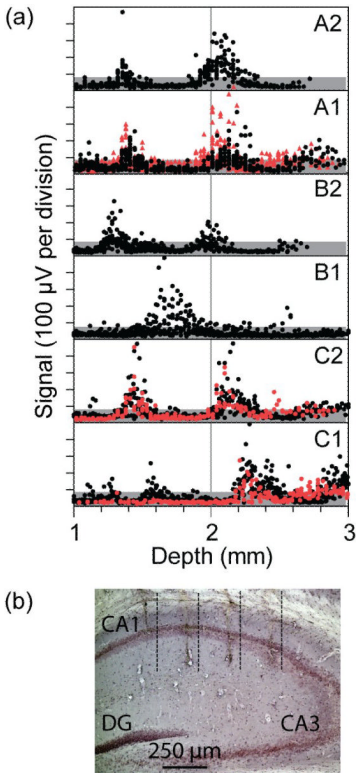

Fig. 3.

(a) Signal values (mean negative peak of the ten largest spike-like events in a 200 s block) as a function of estimated electrode depth at which they were recorded (relative to bregma). Each labeled box represents a separate penetration from a 1×64 probe, with the label representing the animal name and penetration number; e.g., B2 indicates the second penetration for mouse B. Signal values shown in red were observed during the probe's ascent out of the brain; most values (black) correspond to probe insertion. Data were collected from several animals, with 1–4 penetrations per animal at various AP and ML coordinates. (b) Nuclear stain of a hippocampal tissue slice, showing four parallel probe tracks straddling the CA1 layer. A dashed line is placed to the right of each track for illustration purposes. The tracks were made by the 4×16 probe, and presumably extend to additional cell body layers, either CA3 or dentate gyrus (DG), after leaving the plane of the section.

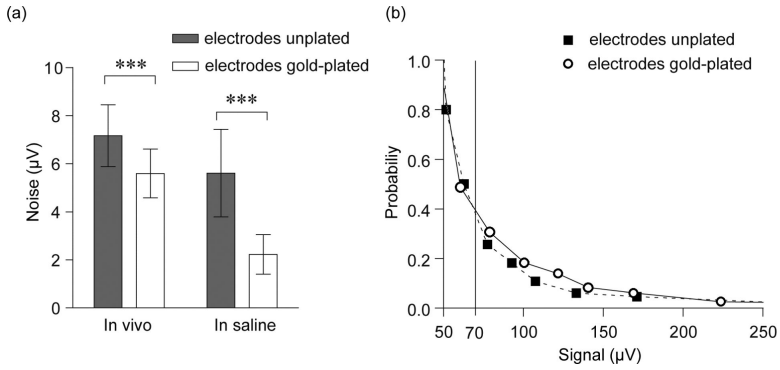

Fig. 4.

Electroplating reduces noise but not signal amplitudes. (a) Mean noise measurements observed on the probe before and after plating, both in the brain and in saline. Error bars denote standard deviation across the included measurements. (b) Empirical probability density function of signal measurements from the same 4×16 probe before and after electroplating. Each point represents a histogram bin center (signal amplitude) and the count normalized by the size of the bin. The vertical line at 70 μV demarcates the designated threshold for spike classification.

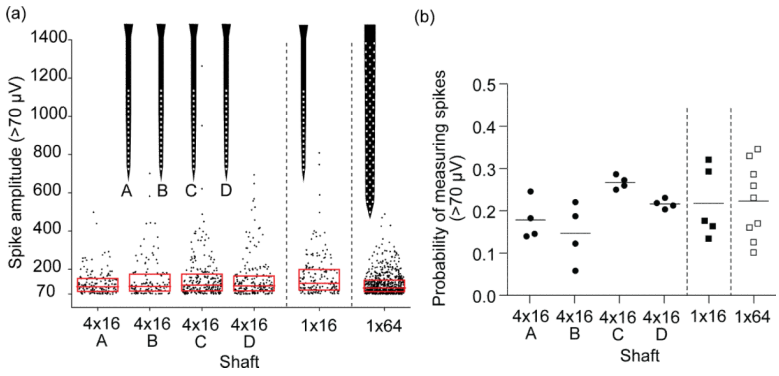

Fig. 5.

Variability of spike amplitude by probe type. (a) Each point represents the spike amplitude on one channel during one recording block. Lines are at the median spike amplitude and boxes extend from the 25th to 75th percentile. The 1x16 geometry refers to shaft C of the 4×16 probe after physically breaking the other three shafts. To account for differences in length spanned by the probes, sites on the 1×64 probe further than 620 μm from the tip were excluded from this analysis. The median spike amplitudes shown are 109 μV (4×16A), 111 μV (4×16B), 118 μV (4×16C), 113 μV (4×16D), 127 μV (1×16), and 102 μV (1×64). (b) Comparison of penetration-wise spike yield from various probe geometries. Each point represents the fraction of recordings with signal measurements >70μV, grouped by probe type Horizontal lines denote mean values.

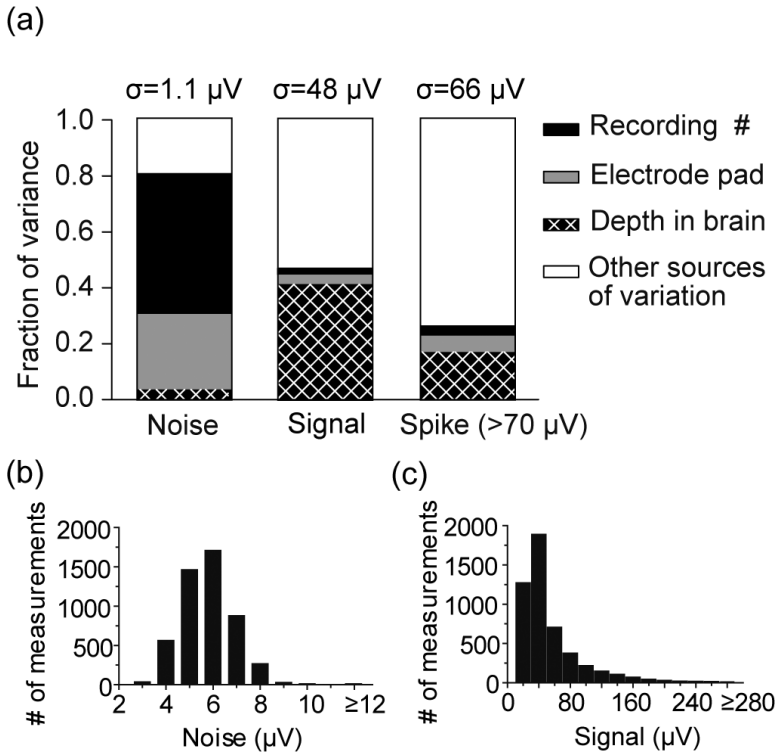

Fig. 6.

Sources of variability in noise and signal measurements with silicon probes. (a) Normalized variance components corresponding to random effects used in ANOVA on noise, signal, and spike amplitude. Spike amplitudes are simply those signal measurements exceeding 70 μV. Variance due to recording and penetration numbers is pooled into `depth in brain'. Sigma values above each bar represent total standard deviation of the set of measurements. (b) Histogram of noise measurements from 1×64 probes included in ANOVA. (c) Histogram of signal measurements from 1×64 probes included in ANOVA.

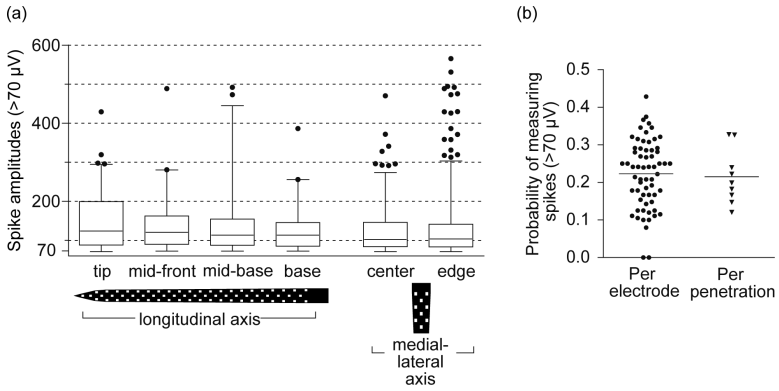

Fig. 7.

Variation in spike amplitude and recording yield with silicon probes. (a) Spike amplitudes (signal measurements exceeding 70 μV) organized by position on the 1×64 probe. The line denotes the median spike amplitude, the box edges are at the 25th and 75th percentiles, and the whiskers extend to the 5th and 95th percentiles. Channels were divided into four groups along the longitudinal axis. In each longitudinal group, only recordings from site depths reached by the entire probe were included in order to account for the effect of location in the brain. The same group of spike amplitude measurements was also plotted based on lateral position in order to compare measurements from central channels ("center") to those from either side ("edge"). Because the same depths in the brain were attained by center and edge channels, recordings from all depths were included. (b) Probability of observing a spike (>70 μV) using a 1×64 probe, organized by channel number and by penetration. Only recordings from site depths obtained by the entire probe were included in computing probabilities per channel, as for the longitudinal groups in (a).